Zhang, Y.; Ren, J.; Zhang, W.; Wu, J.:

Importance of salinity-induced stratification on flocculation in tidal estuaries.

In: Journal of Hydrology. Vol. 596 (2021) 126063.

First published online by Elsevier: 11.02.2021

https://dx.doi.org/10.1016/j.jhydrol.2021.126063

Importance of salinity-induced stratification on flocculation in tidal estuaries

Ying Zhang[a,b], Jie Ren[a,b,*], Wenyan Zhang[c], Jiaxue Wu [a,b,*]

[a]*Center for Coastal Ocean Science and Technology (CCOST), School of Marine Sciences, Sun Yat-sen University, Guangzhou 510275, China.*

[b]*Southern Marine Science and Engineering Guangdong Laboratory (Zhuhai)，Zhuhai 519000, China.*

[c]*Institute of Coastal Research, Helmholtz-Zentrum Geesthacht, Geesthacht, 21502, Germany*

Abstract

Flocculation of suspended particles in tidal estuaries exhibits large spatiotemporal variability due to an interplay of various physical and biogeochemical drivers. Salinity (*S*) is known to promote flocculation of fine-grained suspended particulate matter (SPM). However, the influence of salinity and salinity-induced stratification on flocculation has not been sufficiently investigated yet. This study aims to understand how these two factors, interactively with turbulent shear (*G*) and SPM concentration (*C*), control the vertical variation of floc size and flocculation process in different depth layers in a typical tide-dominated estuarine environment. Analysis of field observation data shows that flocculi (diameter < 20 μm) are mainly affected by *C* and originate primarily from local resuspension. Macroflocs (> 200 μm) are mainly controlled by stratification

---

Abbreviations: ADP, Acoustic Doppler Profiler; ADV, Acoustic Doppler Velocimeter; LISST, Laser In Situ Scattering and Transmissometry; OBS, Optical Backscatter Sensor; PSD, Particle Size Distributions; SPM, Suspended Particulate Matter

*Corresponding authors at:

[a]School of Marine Sciences, Sun Yat-sen University, No. 135, Xingang Xi Road, Guangzhou 510275, China.

E-mail addresses: renjie@mail.sysu.edu.cn (J. Ren); wujiaxue@mail.sysu.edu.cn (J. Wu).

that greatly improves aggregate collision efficiency; Microflocs (20-200 μm), as a transition group between flocculi and macroflocs, are affected by dynamics of both sides. They are influenced jointly by *C*, *G* and stratification. Besides, the fresh water-dominated surface layer is dominated by small particles (flocculi and microflocs), confined in a relatively narrow particle size range between *O* (10^0) and *O* (10^1) as a result of the low level of both *C* (13-20 mg/L) and *S* (< 2 practical salinity units). Below the surface layer, floc size increases drastically along with an increased salinity-induced density gradient and achieves maximum particle size (*O* (10^2)) within the stratified layer. Because of its high efficiency in promoting flocculation and formation of macroflocs, the stratified layer around the halocline can be regarded as an optimal flocculation zone. The benthic layer is characterized by high *C* (> 30 mg/L), gentle *G* (~5/s), and periodic stratification, which result in a wide size range between *O* (10^1) and *O* (10^2) with microflocs as the dominant group. Finally, we found that the accuracy of flocculation modeling can be significantly improved by integrating a simple relationship between particle collision and stratification.

Keywords: SPM dynamics; optimal flocculation zone; benthic layer; halocline; particle collision

1. Introduction

Fine-grained suspended particulate matters (SPM) often aggregate to form larger and porous flocs in estuaries, resulting in a constant change of their properties such as size, density, and settling velocity during their transport (Droppo, 2001; Shen et al., 2018). On the other hand, estuaries are often characterized by highly variable hydrodynamic and biogeochemical environments that are modulated by tides and/or waves. The high sensitivity of SPM dynamics (flocculation/deflocculation) to change of hydrodynamic (e.g. turbulent shear (G) and the stratification induced by salinity and/or temperature gradient) and biogeochemical (e.g. organic/inorganic content, ionic strength, and extracellular polymeric substances) conditions impedes a comprehensive understanding of SPM dynamics and floc size distribution at both temporal and spatial scales (Guo et al., 2017; Lai et al., 2018; Mietta et al., 2009a).

Once flocculated, the size of flocs can vary over several orders of magnitude, namely from 10^0 to 10^3 μm (Thomas. et al., 1999), and accordingly, flocs can be classified into three size groups, namely flocculi (< 20 μm), microflocs (20–200 μm) and macroflocs (> 200 μm) (Fettweis et al., 2012, 2017; Lee et al., 2012, 2014). Compact flocculi are regarded as the basic building blocks of aggregates because they mainly consist of strongly bound clay minerals (Leussen, 1994). Flocculi flocculate rapidly to form microflocs with a regular shape and smooth surface when favorable conditions for flocculation are met (He et al., 2012). Elongated and highly porous macroflocs are ultimately formed from flocculi and microflocs during low turbulence periods (Winterwerp and Kesteren, 2004).

Each particle group has unique physicochemical properties and a corresponding flocculation mechanism. Based on the fractal theory, an inverse relationship exists between floc size and excess density of flocs ($\rho_{f,e}$, with reference to water density, ρ_w). (Mikkelsen et al., 2006; Verney et al., 2011). The $\rho_{f,e}$ of the three groups differs significantly. It varies between 70 and 1000 kg/m^3 for flocculi, between 20 and 200 kg/m^3 for microflocs and normally less than 20 kg/m^3 for macroflocs, respectively (Maggi, 2007; Manning and Dyer, 1999). With low $\rho_{f,e}$ values, macroflocs normally contribute the least amount of the total SPM mass weight in coastal waters, whilst the proportions of microflocs and flocculi are in ascending order (Lee et al., 2016).

The strength of flocs is also highly correlated to their size (Jarvis et al., 2005; Son, 2009). Regardless of biological factors, macroflocs are most sensitive to change in turbulent shear *G*, i.e. they are more likely to be destroyed by strong *G* (e.g. > 12/s) and conversely promoted by gentle *G* (Lee et al., 2011, 2012; He et al., 2012; Mikkelsen et al., 2006). The impact of SPM concentration (*C*) on flocculation is not straightforward. The classic aggregation theory assumes that an increase of *C* would enhance flocculation by increasing the collision frequency (Cross et al., 2013; Hill, 1998). However, other studies have revealed that this assumption can only be satisfied in quiescent water and/or at low *C*, and the enhancement would cease when *C* reaches above a certain level (e.g. 280 mg/L) (Dyer, 1989; Leussen, 2011; Oles, 1992; Zhang et al., 2020). As for the effect of vertical gradient of *C*, it enhances settling velocity of flocs usually under low shear conditions (e.g. *G* <= 0.72/s) and is negligible in an estuarine environment (Cuthbertson et al., 2010).

The influence of salinity (S) and salinity-induced stratification on flocculation are less understood compared to that of C and G. The impact of S is twofold. It affects flocculation in both chemical (particles surface charge) and physical (stratification) ways. In a chemical way, salinity can change electrokinetic properties and zeta-potential of particles, thereby affecting collision efficiency (k_A) between particles. Three modes of flocculation response to salinity can be drawn from literature: 1) Mode 1 corresponds to a constantly positive correlation between k_A and S, 2) Mode 2 refers to an initial positive correlation between k_A and S until S reaches a critical salinity (S*), and then k_A remains steady along with a further increase of S, and 3) Mode 3 represents a range of optimum salinity within which k_A reaches peak value and drops outside the range. The proper mode in estuary, however, depends on clay mineral and seawater compositions (Mietta et al., 2009b; Quezada et al., 2018, 2020; Shen and Maa, 2016). The physical impact of S on flocculation through stratification is to hinder the exchange of SPM across the halocline, thereby trapping particles and resulting in increased frequency of aggregate collision and attachment (Lee et al., 2016; Ren and Wu, 2014; Xia et al., 2004). Hence, it can be concluded that the role of S lies in a change of k_A between particles, however, a quantitative dependency of k_A on S is missing in either way. Besides, S has yet to be considered in the flocculation model although its importance has been well recognized (Lai et al., 2018; Liu et al., 2018; Winterwerp, 1998).

Because the particle settling velocity is dependent on the floc size, vertical distribution of floc size is crucial to evaluate the settling flux of particles. However, this issue is puzzled by the complexity of physical and biogeochemical environmental factors in situ (Sherwood et al., 2018; Strom and Keyvani, 2016). Contradictory results have been derived concerning the change in floc

size associated with water depth based on in situ observations (Eisma et al., 1994; Fugate and Friedrichs, 2003; Papenmeier et al., 2014; Sahin, 2014). Because of hydrological factors that adjust with tidal flows in tide-dominated estuaries, vertical variability of particles has been classified based on tidal phases (Figueroa et al., 2019; Guo et al., 2017; Manning et al., 2006). Floc size has been reported to coarsen downward during the stratified ebb or slack waters, and be homogenous during the well-mixed flood or peak flows (Figueroa et al., 2019; Guo et al., 2017). However, opposite case, i.e. larger particles in the upper river plume, has also been observed (Lee et al., 2016; Li et al., 2017). These results suggest that stratification plays an important role in controlling SPM dispersal and floc size distribution on the vertical plane, although a quantitative relationship between the floc size and stratification is missing. Further, flocculation in and around the benthic layer show even higher complexity because of the unique hydrodynamic structure and active processes of settling and resuspension there (Eisma, 2012). For instance, nepheloid layers characterized by high turbidity and larger flocculated particles have been found in the benthic layer (Li et al., 2017; Zhang et al., 2018).

Furthermore, the importance of numerical models to predict the transport and fate of cohesive sediments has been widely recognized (Jeldres et al., 2018; Thomas. et al., 1999). In general, there are three types of flocculation models, including the extended Lattice Boltzmann Model (Zhang et al., 2013), Population Balance Model (Lee et al., 2011; Maggi et al., 2007; Shen et al., 2018), and Winterwerp flocculation model (Winterwerp, 1998). The Winterwerp model is used to predict a single and dynamic characteristic floc size, with a consideration of the impacts of G, C, and inherent floc properties (Winterwerp, 1998). It has been widely used because of its high

computational efficiency and easy integration into hydrodynamics models (Kuprenas et al., 2018; Winterwerp and Kesteren, 2004).

Based on in situ measurements in the Pearl River Estuary, we aim to address the knowledge gap in understanding how *S* and *S*-induced stratification, interactively with turbulent shear (*G*) and SPM concentration (*C*), control the vertical variation of floc size and flocculation process in different depth layers in a typical tide-dominated estuarine environment. Based on the observations, we propose a simple relationship between particle collision and *S* to improve existing flocculation models.

2. Materials and Methods

2.1. Regional Setting and field measurements

The Pearl River Delta is presented by a complicated river network that delivers ~1.0×10^7 t/a of sediment load into the South China Sea through eight main outlets (Fig. 1a and 1b, see also http://www.mwr.gov.cn/sj/#tjgb). Hydrodynamics of this study area is characterized by irregular semidiurnal tides with apparent salinity, current velocity, and turbidity cycles. Two sites with contrasting salinity conditions, namely H1 (113°38.288′ E, 22°29.345′ N) and M1 (113°28.016′ E, 22°04.529′ N) located in Hengmen and Modaomen outlets, respectively, were selected to investigate the flocculation process. Both sites are characterized by shallow water having a similar averaged depth of ~6.5 m. Site H1 is mainly controlled by freshwater and affected by diluted water in a well-mixed state during low tide periods (tidal amplitude = 1.38 m). On the contrary, site M1 is featured by stable halocline due to strong river discharge and weak tidal mixing (tidal amplitude = 0.8 m) (Fig. 2).

Fieldwork for recording Particle Size Distributions (PSDs), current, turbidity, and salinity was conducted continuously covering four complete semi-diurnal tides between August 18–20, 2019, and August 21–23, 2019 at the two sites, respectively. Three instrument packages were employed, including a shipboard downward-looking 1 MHz Nortek Acoustic Doppler Profiler (ADP, cell size = 30 cm), a on board steel frame (Fig. 1c), and a benthic quadrupod (Fig. 1d). Specifically, a Sequoia Laser In Situ Scattering and Transmissiometry (LISST-200X) and an Optical Backscatterance Sensor (OBS-3A) were tied together in the steel frame. They were lowered through the water column in a steady speed of ~0.1 m/s at an hourly interval, sampling at 1 Hz, with the aim to record high resolution vertical data of PSD, turbidity, and salinity. Meanwhile, water samples were collected and filtered by pre-weighed filters for calibration of turbidity and SPM concentration. The measuring instruments on the quadrupod included a LISST-200X (sampling frequency = 1 Hz, mounted at 1.35 m above the bed (mab)), an Acoustic Doppler Velocimeter (ADV) for measuring turbulence (32 Hz, 0.5 mab), an OBS-3A (2 Hz, 0.55 mab) for high temporal resolution observation, and an upward-looking ADP (cell size = 30 cm, mounted at 2.1 mab) and a downward-looking high resolution ADP (5 cm, 1.75 mab), together with the shipboard ADP, were all configured to provide average values for every 10-min interval, with the aim to provide a detailed vertical structure of currents.

The LISST-200X was able to record PSDs in 36 logarithmically spaced size groups over the range 1–500 μm (Agrawal and Pottsmith, 2000). However, its performance is affected by high turbidity conditions (Guo et al., 2017). To overcome this problem, the Path Reduction Module, which reduces the optical path from 25 mm to 5 mm and thereby increasing the maximum

concentration by a factor of 5 (sequoiasci.com), was equipped with the LISST on quadrupod. Therefore, high frequency and stable measurements of benthic flocculation can be satisfied.

2.2. Data Processing

2.2.1. Turbulent shear

Turbulent shear rate (G) is defined as:

$$G = v/\eta^2 = \sqrt{\epsilon/v}\ (/\mathrm{s}), \quad (1)$$

where v is the kinematic viscosity of the fluid, η is the Kolmogorov microscale and ϵ is the turbulent energy dissipation rate. The values of ϵ can be obtained from the Turbulence Kinetic Energy (TKE) spectra (Guerra and Thomson, 2017), which is transformed from the fluctuated velocity recorded by ADV (32 Hz). The TKE spectra method is based on the Kolmogorov hypothesis, i.e. energy transfer is determined solely by ϵ in the inertial subrange (Kolmogorov, 1941; Pope, 2000). However, the quality of the ADV data is affected by the occasional disturbance caused by Doppler noise, high SPM concentration, or weak Doppler signal during slack waters (Goring and Nikora, 2002; Wu et al., 2011), which obscure the inertial subrange in TKE spectra and impede the validity of G solving. To derive continuous time series of G, a three-step procedure was applied in this study.

Firstly, TKE spectra were estimated from the high-frequency velocity (32 Hz) and then the inertial subrange was determined through an automated searching technique (Zhang et al., 2020). Secondly, data quality was controlled by the slope of the spectra in the presence of inertial subrange. According to the Kolmogorov hypothesis, the slope should be around -5/3. In this study, a slope within a range of -5/3$\pm$20% was considered to indicate good quality data. Data beyond

this range was regarded unusable. The final step was to establish a relationship between *G* and the corresponding mean flow velocity (*U*) for every 10-min interval. It is assumed that a proportional relationship exists between ϵ and cube of friction velocity u_* (Eq. 2) (Nakagawa and Nezu, 1993), and between u_* and *U* (Eq. 3) (Kuprenas et al., 2018). Combining the definition of *G*, the relationship can be derived (Eq. 4).

$$\epsilon \propto {u_*}^3, \quad (2)$$

$$u_* \propto U, \quad (3)$$

$$G = K\sqrt{|U^3|/\nu}, \quad (4)$$

where *K* is a constant. Based on measured *U* and valid *G* from ADV data, the value of *K* = 0.0502 (0.0316) with correlation coefficient *r* = 0.84 (0.82) for site H1 (M1) was obtained. The value is of the same order of 0.075 proposed by Kuprenas et al. (2018). Thereafter, continuous values of *G* in the bottom layer could be estimated from *U* averaged from the ADV.

2.2.2. Floc properties

The LISST-based raw data need to be pre-processed before deriving PSDs (for details see Zhang et al. (2020)). To eliminate the influence caused by turbulence bursting in the benthic layer, such as short-term vertical sediment transport and variations of PSDs (Mikkelsen and Pejrup, 2001), a local outlier factor detection (Breunig et al., 2000) was applied.

Two methods were adopted to obtain the volumetric concentration (VC) of the three floc size groups, i.e. flocculi, microflocs, and macroflocs. The first method is to separate PSDs directly by the empirically critical diameter values, D_{sp} (Mikkelsen et al., 2006). Values of D_{sp} between

flocculi and microflocs, and between microflocs and macroflocs, were selected as 20 and 200 μm, respectively (Lee et al., 2012; Winterwerp and Kesteren, 2004). The second method assumes that the PSDs in coastal waters can be decomposed into lognormal size classes. It has the advantage of providing more detailed information, e.g. the representative size and standard deviations (σ), about the unimodal PSDs of each group than the first method (Fettweis et al., 2012; Lee et al., 2012). But this approach is much more expensive in terms of computational cost. In our study, the second method was performed only when analyzing detailed PSDs in the selected vertical profiles (see section 3.4), and the first was applied in other cases. It is worth to note that the VC of each group resolved from the two methods have similar trends, despite the slight differences in the exact values (e.g. r = 0.89 and RMSD = 14% for benthic macroflocs at site H1). Therefore, the choice of method does not affect the overall validity of the results.

The mean diameter of flocs can be expressed in various ways (Shen, 2016), such as D_{32} (area-weighted diameter), D_{43} (volume-weighted diameter), D_{60} (hydrodynamic mean size), and D_{50} (median size). Among these parameters, D_{32} is concerned with surface area and has been adopted by LISST-25 instrument (Agrawal and Mikkelsen, 2009; Filippa et al., 2012). Considering the impact of salinity is associated with particle surface properties (e.g. charge and cohesiveness), D_{32} was selected to be the representative diameter in this study.

2.2.3. Definition of three depth layers

To help interpret the data, the whole water column is divided into three vertical layers in our analysis based on observation. The surface layer is defined as $S < 2$ practical salinity units (psu) and water density gradient $d\rho_w/dz < 2$ kg/m^4. Here, the suffix psu, equivalent to units of parts per

thousand, is used to indicate salinity values of electrical conductivity measurements (Lewis and Perkin, 1978). The stratified layer is defined as $d\rho_w/dz \geq 2$ kg/m^4. The benthic layer is defined as the water beneath the stratified layer. Note that the three defined layers were not always persistent at the two sites due to the change of mixing states by tides, e.g. the benthic layer was taken over by the stratified layer during ebb tides at M1, while the water column was completely occupied by the surface layer during ebb tides at H1.

2.3. Numerical modelling of flocculation

Assuming $n_f = 2$ in this work which is commonly used in the literature (Maggi et al., 2007; Winterwerp, 1998), in the modified Winterwerp model proposed by Kuprenas et al. (2018, referred to K18 hereafter), the rate equation for mean diameter of flocs (D) can be simply expressed as:

$$dD/dt = 1/2[k_A GCD^2/(\rho_P D_P) - k_B DG(D - D_P)\left(\mu GD^2/F_y\right)^q/D_P], \quad (5)$$

where D_p is the size of primary particles, μ is the dynamic viscosity of the fluid, F_y is the floc yield strength, and k_B is breakup efficiency of flocs. Coefficients of k_A and k_B are related to the physicochemical properties of particles and water (Leussen, 1994; Winterwerp, 1998). Since quantitative information about the two coefficients is unavailable, they are normally treated as fitting parameters in the model (Leussen, 1994, 2011; Shen et al., 2018). The coefficient q is given by:

$$q = c_1 + c_2 D/\eta, \quad (6)$$

where c_1 and c_2 are constant coefficients, defined as 0.5 and 1.5, respectively. The setting of c_1 and c_2 is to limit the size of the floc to Kolmogorov microscale, thereby improving the modelling performance across a wide range of concentrations (Kuprenas et al., 2018).

The key state variables in the K18 model include the particle size, the mass SPM concentration, and the turbulent shear. The impact of salinity and stratification is implicitly incorporated into the value of k_A. In this study, we propose a simple parameterization of k_A by including its explicit dependence on S and stratification. Time series of the state variables including S derived from the field measurements were fed into the model to evaluate the flocculation process.

3. Results

3.1. Hydrodynamic conditions

The mean SPM concentrations measured from the survey were 31 and 22.5 mg/L at site H1 and M1, respectively (Fig. 2c and 2g). These two sites were also similar in current strength, such as fluctuation range (between -1.12 and 0.8 m/s at H1 and between -1.14 and 0.64 m/s at M1) and maximum vertical averaged velocity (-0.83 and -0.89 m/s at H1 and M1, respectively; Fig. 2d and 2h). However, the salinity condition differed significantly between the two sites.

Site H1 was characterized by a weak halocline (0.34 psu/m on bulk average) that was periodically disturbed by tides (Fig. 2b). Freshwater dominated during low tide periods, and brackish water intruded this site in a partly-mixed state following flood tides with maximum S = 9 psu at high water level (Fig. 2a).

In contrast to the weak and unstable stratification at H1, site M1 showed a persistent highly stratified state with a distinct band-shaped halocline throughout the observation periods (Fig. 2f). The surface and benthic layers were occupied by freshwater (< 2 psu) and saline water (> 13 psu), respectively (Fig. 2e). In between was the stratified layer distributed within the range of S = 2-13 psu (Fig. 2e and 2f). In this stratified layer, dS/dz = 4.1 psu/m and $d\rho_w/dz$ = 3 kg/m^4; and in other parts of the water column, dS/dz < 1.4 psu/m and $d\rho_w/dz$ < 1 kg/m^4. The stratified layer fluctuated vertically with the water level (r = 0.87) with an average depth of 3.2 m at its center and occupied 35% of the whole water column with an average thickness of 2.27 m.

Resuspension of seafloor sediment occurred at both sites, but in different forms (Fig. 2c and 2g). The vertical diffusion of resuspended sediment at site H1 was featured by a uniform C in the vertical plane (Fig. 2c), but at M1, it was confined below the stratified layer, e.g. C is reduced to less than 30 mg/L above 3 mab (Fig. 2g).

Regarding the vertical velocity structure (Fig. 2d and 2h), current strength was more uniform at site H1 (σ = 0.1 m/s) than that at M1 (σ = 0.17 m/s). In contrast to a vertically-uniform flow structure at H1, site M1 was featured by baroclinic flows with the highest flow velocity appearing in the mid-water depth. The duration of ebb and flood in the benthic layer was approximately the same at both sites, whereas ebb flows dominated in the surface layer accounting for 78% length of time at M1.

Meteorological forcing (winds and waves) for the monitoring period was monitored, but proved to be negligible for our analysis, because they are too weak to influence hydrodynamics and flocculation. Significant wave heights measured at 1.7 mab were persistently smaller than

0.12 m at both two sites. The winds were also weak, with averaged speed of 1.5 and 2.2 m/s at site H1 and M1, respectively.

3.2. Flocculation zone

At site H1, intensified flocculation with large particle size and VC occurred at the interface between freshwater and brackish water at high water slacks where S > 2 psu (Fig. 3a and 3b). Particle VC in the region of S > 2 psu accounted for ~70% of the total particle VC and was characterized by a larger average diameter (D = 38 μm) than that in freshwater (D = 28 μm). When freshwater occupied the water column at low water levels, flocs were almost smaller than 40 μm and a mild downward coarsening trend was seen in the particle size distribution. Particles in the low water level periods were more homogeneously distributed (D = 27±11 μm) in the vertical plane than that during the high water (D = 37±32 μm; Fig. 3a and 3b).

At site M1, intensive flocculation appeared in the stratified layer. Particles in this layer also accounted for ~70% of the total VC. On the other hand, they were more than twice larger (D = 90 μm) but much lighter ($\rho_{f,e}$ = 73.8 kg/m^3) than those in the surface and benthic layers (D = 41 μm and $\rho_{f,e}$ = 308 kg/m^3; Fig. 3c and 3d). In contrast to the periodical formation and destruction at H1, large flocs at M1 were persistently observed throughout the tidal cycles.

The region of S > 2 psu and the stratified layer at the two sites appeared to provide the optimal condition for flocculation. Large flocs are scattered in these flocculation zones. A critical value of S* = 2 psu (referring to Mode 2) for flocculation can also be concluded, which was in agreement with experiment results, e.g. S* <= 5 psu (Zhang et al., 2019). On the other hand, the size of flocs (D = 90 μm) and their VC (= 357 μL/L) in the stratified layer at site M1 were much

larger than those in the region of S > 2 psu at H1 (D = 38 μm and VC = 205 μL/L), which indicates the importance of stratification on flocculation.

3.3. Distribution of floc size

To investigate the spatiotemporal distribution of floc size, VC of the three size groups, namely flocculi (< 20 μm), microflocs (20–200 μm), and macroflocs (> 200 μm), was calculated, respectively (Fig. 4). Results indicate that the VC of flocculi was closely correlated with C (r = 0.74) at both sites (Fig. 4a and 4d). Compared to a more vertically-uniform distribution at site H1, flocculi at M1 were mostly confined below the stratified layer. The average VC of flocculi at M1 above 3 mab was 13 μL/L, which is merely 28% of that in the benthic layer. Microflocs at site H1 also showed a strong correlation with C (r = 0.71), with higher values of VC appearing near the benthic (Fig. 4b). However, at site M1, 42% of microflocs were scattered within the flocculation zone (i.e. the stratified layer), whereas 47% were confined in the benthic layer and correlated with C (Fig. 4e). Large portions of macroflocs were concentrated in the flocculation zone at both sites, accounting for 30% (H1) and 64% (M1) of total VC in the water column, respectively (Fig. 4c and 4f). The relationships between each size group and environmental factors suggest that flocculi are mainly determined by C that primarily originates from local resuspension, whereas macroflocs are largely controlled by stratification and promoted by salinity. Microflocs, as a transition group between flocculi and macroflocs, are affected by both sides. They are influenced by not only C but also strong stratification.

3.4. Impact of stratification on flocculation

With a favorable condition for flocculation (see section 3.2), vertical profiles at site M1 around high slack tides (t = 15 h) were analyzed in further detail. Results show that the stratified layer was featured by large particles with a wide size range (Fig. 5a). The mean and standard deviation values of particle size in the stratified layer were 150 and 102 μm, respectively, notably larger than those (D = 22 μm and σ = 8 μm) in other parts (i.e. the surface and benthic layers) of the water column. VC of particles in the stratified layer was 1077 μL/L, being more than 10 times of the value in the benthic layer (103 μL/L) and 80 times of that in the surface layer (13 μL/L). On the other hand, $\rho_{f,e}$ in the stratified layer (73.8 kg/m^3) was less than a quarter of that outside the stratified layer (= 308 kg/m^3).

PSDs at three heights (H = 1.8, 5, and 6.5 mab, respectively) representing each depth layer were calculated to investigate the general patterns in the three layers. Results showed that both the surface and benthic layers exhibited a bimodal structure, while the stratified layer presented a unimodal distribution (Fig. 5b). The bimodal structure in the PSD of the surface layer was characterized by a similar distribution of flocculi and microflocs, with diameters of 6.7 and 28 μm, respectively, whereas macroflocs were absent. The stratified layer was occupied by macroflocs with a diameter of 334 μm, accounting for as high as 90% of the total VC of particles. Particles were dominated by flocculi and microflocs again in the benthic layer, accounting for 36% and 64% of the total VC of particles with diameters of 18.7 and 130 μm, respectively. Compared to the wide range of PSD of each size group (σ = 1.93) in the surface and benthic layers, PSD was confined within a narrow range in the stratified layer with σ = 1.13.

These significant differences between the stratified layer and its outside reveal that stratification greatly promotes flocculation, resulting in concentrated PSD dominated by larger particles with higher VC and lower $\rho_{f,e}$ than that in the unstratified water column.

3.5. Flocculation modelling

Based on our analysis of field data, a simple parameterization scheme of collision efficiency of particles (k_A) by including its explicit dependence on S (referring to Mode 2) and stratification ($d\rho_w/dz$) was applied in the K18 model, which is expressed as:

$$k_A = \min\left\{\left(k_1 + f(S) + f\left(\frac{d\rho_w}{dz}\right)\right), 1\right\}, \quad (7)$$

$$f(S) = \begin{cases} k_2 S & if\ S < S^* \\ k_2 S^* & if\ S \geq S^*, \end{cases} \quad (8)$$

$$f\left(\frac{d\rho_w}{dz}\right) = k_3 * \frac{d\rho_w}{dz}, \quad (9)$$

where maximum of k_A = 1 is adopted to meet its physical definition (Kuprenas et al., 2018; Winterwerp, 1998; Zhang et al., 2020). Parameters of k_1, k_2, and k_3 are positive constants, which are derived from the minimum error between the simulated and measured diameter.

Here, S^* = 2 psu in both two sites based on observation (see section 3.2), and the data collected on the quadrupod with high stability and time resolution were tested. For site H1, values of k_1 = 0.1, k_2 = 0, k_3 = 0.15 and k_B = 1E-6 were obtained with r = 0.55 and RMSD = 54.44 μm before 37 h (Fig. 6a and 7a); and for site M1, values of k_1 = 0, k_2 = 0, k_3 = 0.65, and k_B = 7E-6 were derived, with r = 0.67 and RMSD = 37.5 μm before 44 h (Fig. 6g and 7b). Besides, the measured particle size lagged simulated value by ~0.6 h at site H1, which is partly attributed to inconsistent locations of instruments, i.e. LISST-200X (H = 1.35 mab) was above OBS-3A and

ADV (H = ~0.5 mab), as it takes a certain time for resuspended sediment to transport to upper layer (Fettweis et al., 2006). Regarding to the original parameterization scheme (i.e. without dependence of k_A on S and stratification) during same period, for site H1, values of k_A = 0.15 and k_B = 1E-6 were obtained with r = 0.42 and RMSD = 56.14 μm (Fig. 6a and 7a); and for site M1, values of k_A = 0.05 and k_B = 1E-6 were derived, with r = 0.08 and RMSD = 58.7 μm (Fig. 6g and 7b).

Compared to the original parameterization scheme, our new parameterization of collision efficiency k_A proves to be significant and robust (Fig. 7). Values of the coefficients k_A and k_B fall within the range derived in previous research, i.e. k_A = 0.1-1 and k_B = O (10^{-6}) - O (10^{-5}) (Kuprenas et al., 2018; Winterwerp, 1998; Zhang et al., 2020). The advantage of our parameterization, compared to empirical values derived from fitting, is the introduction of a physically-based prediction scheme of k_A through an explicit dependency of particle collision on S and stratification so that the formula (Eq. 7-9) can be applied broadly to estuarine environments.

4. Discussion

4.1. Importance of salinity on flocculation

In an earlier study (Zhang et al., 2020), we have investigated the impact of C and G on flocculation at another two monitoring sites in the Pearl River estuary. Results from the current study further prove the findings from the previous study that evolutions of flocs with different initial sizes synchronize gradually to adapt to the local hydrological environment in each depth layer, and the trends of floc size evolution and absolute net flocculation rates are similar among diverse tidal shear cycles. The impact of stratification was also explored in the previous study but

384 to a less extent than the current study. In the previous study we found that the halocline increases
385 vertical variation of flocs size, and divides the water column into two vertical zones with distinct
386 flocculation dynamics. Flocculation within the stratified layer across the halocline was not
387 investigated due to insufficient data (one site was completely dominated by freshwater whilst the
388 other was dominated by saline water with only a thin and unstable stratified layer near the surface).
389 In this study, the newly derived observation data from site M1 which was featured by a persistent
390 stratified layer allow a further investigation of flocculation dynamics in this layer.

391 Our new observation suggests that the chemical impact of salinity (in the form of surface
392 charge) is much smaller than that of stratification. In stratified states (site M1), the poor
393 performance of modelling without considering stratification (e.g. r = 0.08 and 0.67 for the original
394 and new scheme, respectively; Fig. 7b) confirms that salinity-induced stratification is an essential
395 driver for flocculation, especially for the formation of macroflocs (see also section 3.3).

396 It is worth noting that salinity is also highly correlated to the mixing degree of the river- and
397 sea- born materials, that is, it can be treated as an indicator of physico-chemical proporties of
398 sediment (e.g. mineralogy, electrophoretic mobility, cation exchange capacity, specific surface
399 area) (Leussen, 1994). That suggests the necessity of continuous sampling and component analysis
400 of suspended sediment in future studies.

401 **4.2. Interplay of major influencing factors**

402 To illustrate flocculation pattern in surface layer, data collected at site M1 was analyzed.
403 Flocs size on the surface was quite small in general (D_{50} = 16.5 μm). Macroflocs from flocculation
404 zone were dispersed into surface layer, which coincided with high water level (i.e., t = 13, 25 and

39 h) in weak current environments (e.g. $U < 0.2$ m/s) (Fig. 8). The brief peaks of floc were soon be deflocculated into flocculi and microflocs by subsequent ebb peak flows (e.g. $U > 0.5$ m/s). Afterward, the portion of microflocs increased slowly by the transformation of flocculi (Fig. 8b). The maximum values of SPM concentration were in correspondence to the ebb peak flows (r = 0.71; Fig. 8c), indicating that the surface layer was controlled by upstream freshwater. The weak flocculation in the surface can be attributed to several aspects. Quite small values and fluctuation range of SPM concentration (13-20 mg/L), resulting in insufficient particles, limit flocculation in surface (Hill, 1998). Besides, the negative charges on flocs surface as a result of low salinity can lead to electrostatic repulsion between particles, which impedes their interaction and bonding (Parsons et al., 2016; Quezada et al., 2018).

In the stratified layer, C was higher than that in the surface layer because of input from the benthic layer, however, its time series does not exhibit a significant correlation with floc size (r = -0.45), suggesting that C is not a main controlling factor for flocculation in this layer (Fig. 2 and 3). C in the benthic layer was persistently larger than that in the upper layers due to resuspension during peak tidal flows, with average values of 40.7 mg/L and 33.7 mg/L at H1 and M1, respectively (Fig. 6d and 6j). The elevated C together with mild shear (G = 5/s) (Fig. 6c and 6i) promoted flocculation in the benthic layer (Fig. 6b and 6h), although being less intensive compared to that in the stratified layer (note that the benthic layer was taken over by the stratified layer during ebb tides at M1).

It is also worth noting that volumetric concentration (VC) is not the same as mass concentration (*C*). VC reflects the flocculation status in terms of floc diameter (*D*). The relationship between VC and *D* is:

$$VC = N\left(\frac{\pi}{6}D^3\right), \quad (10)$$

where *N* represents the number of particles. The cube root of VC was positively correlated to *D* at site M1 (r = 0.78; Fig. 9). It is quite interesting and worth to note that *N* differs slightly between the surface and stratified layers while is significantly larger in the bottom layer where mass concentration *C* is much higher.

Besides, tidal cycle of hydrodynamic conditions can lead to both highly variability and periodicity of flocculation. As for site H1 in a partly-mixed state, flocs size in the bottom layer was symmetrical around the moment of the strongest stratification at t = 23 h (Fig. 6a and 6f), with skewness coefficient as low as 0.1. In detrending conditions, the diameters of flocs showed quarter-diurnal periodicity and a negative correlation with *G* (r = -0.65; Fig. 6a and 6c). For site M1 controlled by stratification, flocs decreased/increased during flood/ebb periods and exhibited semidiurnal periodicity of flocculation (Fig. 6g and 6i).

5. Conclusions

Based on in situ observations and modelling, this study investigated how salinity and salinity-induced stratification, interactively with turbulent shear (*G*) and SPM concentration (*C*), control the vertical variation of floc size and the flocculation process in different depth layers in a

typical tide-dominated estuarine environment. According to the results, the following conclusions are drawn.

1. Flocculi are mainly affected by SPM concentration and originate primarily from local resuspension, whereas macroflocs are largely controlled by stratification. Microflocs, as a transition group between flocculi and macroflocs, are affected by dynamics of both sides. They are controlled jointly by SPM concentration, shear rate and stratification.

2. Compared to bimodal PSDs in the surface and benthic layers dominated by small particles (i.e. flocculi and microflocs), the unimodal PSD in the stratified layer is narrow and dominated by macroflocs with high VC and low $\rho_{f,e}$.

3. Because of a high efficiency in promoting flocculation and formation of macroflocs, the stratified layer around the halocline can be regarded as an optimal flocculation zone.

4. Flocculation modelling should consider an explicit dependency of particle collision on stratification.

Author contributions

Conceptualization: J.R., W.Z., W.J., and Y.Z.; Data curation: W.J. and J.R.; Methodology. Y.Z. and J.R.; Modelling: Y.Z. and W.Z.; Investigation: W.J., J.R., and Y.Z.; Original draft: Y.Z. and W.Z.; Writing - review & editing: Y.Z. and W.Z..

Declaration of Competing Interest

The authors declare that they have no known competing financial interests or personal relationships that could have appeared to influence the work reported in this paper.

Acknowledgments

This work was jointly supported by the National Natural Science Foundation of China (NSFC) [Grant number 42076173, U1901209]. W. Zhang acknowledges the support from the research program “Marine, Coastal and Polar Systems” (PACES II) of the Hermann von Helmholtz-Gemeinschaft Deutscher Forschungszentren e.V. We also thank two anonymous reviewers, whose valuable comments contributed significantly to improve this manuscript.

References

Agrawal Y.C., Mikkelsen O.A. (2009) Shaped focal plane detectors for particle concentration and mean size observations. Optics Express 17:23066-23077.

Agrawal Y.C., Pottsmith H.C. (2000) Instruments for particle size and settling velocity observations in sediment transport. Marine Geology 168:89-114.

Breunig M.M., Kriegel H.P., Ng R.T., Sander J. (2000) LOF: Identifying density-based local outliers, Proc. ACM SIGMOD.

Cross J., Nimmo-Smith W.A.M., Torres R., Hosegood P.J. (2013) Biological controls on resuspension and the relationship between particle size and the Kolmogorov length scale in a shallow coastal sea. Marine Geology 343:29-38.

Cuthbertson A.J.S., Dong P., Davies P.A. (2010) Non-equilibrium flocculation characteristics of fine-grained sediments in grid-generated turbulent flow. Coastal Engineering 57:447-460. DOI: 10.1016/j.coastaleng.2009.11.011.

Droppo I.G. (2001) Rethinking what constitutes suspended sediment. Hydrological Processes 15:1-14. DOI: 10.1002/hyp.228.

Dyer K.R. (1989) Sediment processes in estuaries: Future research requirements. Journal of Geophysical Research: Atmospheres 94 (C10):14327-14339.

Eisma D. (2012) Suspended matter in the aquatic environment Springer, Berlin, Heidelberg.

Eisma D., Chen S., Li A. (1994) Tidal variations in suspended matter floc size in the Elbe river and Dollard estuaries. Netherland Journal of Aquatic Ecology 28:267-274.

Fettweis M., Baeye M., Lee B.J., Chen P., Yu J.C.S. (2012) Hydro-meteorological influences and multimodal suspended particle size distributions in the Belgian nearshore area (southern North Sea). Geo-Marine Letters 32:123-137. DOI: 10.1007/s00367-011-0266-7.

Fettweis M., Frederic F., Virginie P., Dries V.D. (2006) Suspended particulate matter dynamics and aggregate sizes in a high turbidity area. Marine Geology 235:63-74.

Fettweis M., Lee B.J. (2017) Spatial and Seasonal Variation of Biomineral Suspended Particulate Matter Properties in High-Turbid Nearshore and Low-Turbid Offshore Zones. Water 9. DOI: 10.3390/w9090694.

Figueroa S.M., Lee G.h., Shin H.J. (2019) The effect of periodic stratification on floc size distribution and its tidal and vertical variability: Geum Estuary, South Korea. Marine Geology 412:187-198. DOI: 10.1016/j.margeo.2019.03.009.

Filippa L., Trento A., Álvarez A.M. (2012) Sauter mean diameter determination for the fine fraction of suspended sediments using a LISST-25X diffractometer. Measurement 45:364-368.

Fugate D.C., Friedrichs C.T. (2003) Controls on suspended aggregate size in partially mixed estuaries. Estuarine Coastal Shelf Science 58:389-404.

Goring D.G., Nikora V.I. (2002) Despiking Acoustic Doppler Velocimeter Data. Journal of Hydraulic Engineering 128:117-126.

Guerra M., Thomson J. (2017) Turbulence measurements from five-beam acoustic doppler current profilers. Journal of Atmospheric and Oceanic Technology 34:1267-1284. DOI: 10.1175/jtech-d-16-0148.1.

Guo C., He Q., Guo L., Winterwerp J.C. (2017) A study of in-situ sediment flocculation in the turbidity maxima of the Yangtze Estuary. Estuarine, Coastal and Shelf Science 191:1-9. DOI: 10.1016/j.ecss.2017.04.001.

He W., Nan J., Li H., Li S. (2012) Characteristic analysis on temporal evolution of floc size and structure in low-shear flow. Water Res 46:509-20. DOI: 10.1016/j.watres.2011.11.040.

Hill P.S. (1998) Controls on floc size in the Sea. Oceanography 11:13–18. DOI: 10.5670/oceanog.1998.03

Jarvis P., Jefferson B., Gregory J., Parsons S.A. (2005) A review of floc strength and breakage. Water Res 39:3121-37. DOI: 10.1016/j.watres.2005.05.022.

Jeldres R.I., Fawell P.D., Florio B.J. (2018) Population balance modelling to describe the particle aggregation process: A review. Powder Technology 326:190-207. DOI: 10.1016/j.powtec.2017.12.033.

Kolmogorov A.N. (1941) Dissipation of energy in locally isotropic turbulence. Akademiia Nauk Sssr Doklady 32:15-17.

Kuprenas R., Tran D., Strom K. (2018) A shear-limited flocculation model for dynamically predicting average floc size. Journal of Geophysical Research: Oceans 123:6736-6752. DOI: 10.1029/2018jc014154.

Lai H., Fang H., Huang L., He G., Danny R. (2018) A review on sediment bioflocculation: Dynamics, influencing factors and modeling. Science of the Total Environment 642:1184–1200. DOI: 10.1016/j.scitotenv.2018.06.101.

Lee B.J., Fettweis M., Toorman E., Molz F.J. (2012) Multimodality of a particle size distribution of cohesive suspended particulate matters in a coastal zone. Journal of Geophysical Research: Oceans 117(C03014):17. DOI: 10.1029/2011jc007552.

Lee B.J., Toorman E., Fettweis M. (2014) Multimodal particle size distributions of fine-grained sediments: mathematical modeling and field investigation. Ocean Dynamics 64:429-441. DOI: 10.1007/s10236-014-0692-y.

Lee B.J., Toorman E., Molz F.J., Wang J. (2011) A two-class population balance equation yielding bimodal flocculation of marine or estuarine sediments. Water Research 45:2131-45. DOI: 10.1016/j.watres.2010.12.028.

Lee J., Liu J.T., Hung C.-C., Lin S., Du X. (2016) River plume induced variability of suspended particle characteristics. Marine Geology 380:219-230. DOI: 10.1016/j.margeo.2016.04.014.

Leussen V. (1994) Estuarine macroflocs and their role in fine-grained sediment transport, (Ph.D. Dissertation) Universiteit van Utrecht, Netherlands.

Leussen W.V. (2011) Macroflocs, fine-grained sediment transports, and their longitudinal variations in the Ems Estuary. Ocean Dynamics 61:p.387-401.

Lewis E.L., Perkin R.G. (1978) Salinity: Its definition and calculation. Journal of Geophysical Research: Oceans 83:466-487.

Li D., Li Y., Xu Y. (2017) Observations of distribution and flocculation of suspended particulate matter in the Minjiang River Estuary, China. Marine Geology 387:31-44.

Liu D., Edraki M., Berry L. (2018) Investigating the settling behaviour of saline tailing suspensions using kaolinite, bentonite, and illite clay minerals. Powder Technology 326:228-236. DOI: 10.1016/j.powtec.2017.11.070.

Maggi F. (2007) Variable fractal dimension: A major control for floc structure and flocculation kinematics of suspended cohesive sediment. Journal of Geophysical Research 112 (C07012). DOI: 10.1029/2006jc003951.

Maggi F., Mietta F., Winterwerp J.C. (2007) Effect of variable fractal dimension on the floc size distribution of suspended cohesive sediment. Journal of Hydrology 343:43-55. DOI: 10.1016/j.jhydrol.2007.05.035.

Manning A.J., Bass S.J., Dyer K.R. (2006) Floc properties in the turbidity maximum of a mesotidal estuary during neap and spring tidal conditions. Marine Geology 235:193-211.

Manning A.J., Dyer K.R. (1999) A laboratory examination of floc characteristics with regard to turbulent shearing. Marine Geology 160:147-170.

561 Mietta F., Chassagne C., Manning A.J., Winterwerp J.C. (2009a) Influence of shear rate, organic matter
562 content, pH and salinity on mud flocculation. Ocean Dynamics 59:751-763. DOI:
563 10.1007/s10236-009-0231-4.

564 Mietta F., Chassagne C., Winterwerp J.C. (2009b) Shear-induced flocculation of a suspension of
565 kaolinite as function of pH and salt concentration. Journal of Colloid & Interface Science
566 336:134-141.

567 Mikkelsen O., Pejrup M. (2001) The use of a LISST-100 laser particle sizer for in-situ estimates of floc
568 size, density and settling velocity. Geo-Marine Letters 20:187-195. DOI:
569 10.1007/s003670100064.

570 Mikkelsen O.A., Hill P.S., Milligan T.G. (2006) Single-grain, microfloc and macrofloc volume
571 variations observed with a LISST-100 and a digital floc camera. Journal of Sea Research
572 55:87-102. DOI: 10.1016/j.seares.2005.09.003.

573 Nakagawa H., Nezu I. (1993) Turbulence in Open Channel Flows. Journal of Hydraulic Engineering
574 120:1235-1237.

575 Oles V. (1992) Shear-induced aggregation and breakup of polystyrene latex particles. Journal of
576 Colloid & Interface Science 154:351-358.

577 Papenmeier S., Schrottke K., Bartholomae A. (2014) Over time and space changing characteristics of
578 estuarine suspended particles in the German Weser and Elbe estuaries. Journal of Sea
579 Research 85:104-115.

580 Parsons D.R., Schindler R.J., Hope J.A., Malarkey J., Baas J.H., Peakall J., Manning A.J., Ye L.,
581 Simmons S., Paterson D.M., Aspden R.J., Bass S.J., Davies A.G., Lichtman I.D., Thorne P.D.
582 (2016) The role of biophysical cohesion on subaqueous bed form size. Geophysical Research
583 Letters 43:1566– 1573. DOI: 10.1002/2016GL067667.

584 Pope S.B. (2000) Turbulent flows Cambridge University Press.

585 Quezada G.R., Jeldres R.I., Fawell P.D., Toledo P.G. (2018) Use of molecular dynamics to study the
586 conformation of an anionic polyelectrolyte in saline medium and its adsorption on a quartz
587 surface. Minerals Engineering 129:102-105. DOI: 10.1016/j.mineng.2018.09.025.

588 Quezada G.R., Ramos J., Jeldres R.I., Robles P., Toledo P.G. (2020) Analysis of the flocculation
589 process of fine tailings particles in saltwater through a population balance model. Separation
590 and Purification Technology 237. DOI: 10.1016/j.seppur.2019.116319.

591 Ren J., Wu J. (2014) Sediment trapping by haloclines of a river plume in the Pearl River Estuary.
592 Continental Shelf Research 82:1-8. DOI: 10.1016/j.csr.2014.03.016.

593 Sahin C. (2014) Investigation of the variability of floc sizes on the Louisiana Shelf using acoustic
594 estimates of cohesive sediment properties. Marine Geology 353:55-64.

595 Shen X. (2016) Modeling flocculation and deflocculation processes of cohesive sediments, (Ph.D.
596 dissertation) Virginia Institute of Marine Science, The College of William and Mary, Virginia,
597 USA.

598 Shen X., Lee B.J., Fettweis M., Toorman E.A. (2018) A tri-modal flocculation model coupled with
599 TELEMAC for estuarine muds both in the laboratory and in the field. Water Research
600 145:473-486. DOI: 10.1016/j.watres.2018.08.062.

601 Shen X., Maa J.P.Y. (2016) A camera and image processing system for floc size distributions of
602 suspended particles. Marine Geology 376:132-146. DOI: 10.1016/j.margeo.2016.03.009.

603 Sherwood C.R., Aretxabaleta A.L., Harris C.K., Rinehimer J.P., Verney R., Ferré B. (2018) Cohesive
604 and mixed sediment in the Regional Ocean Modeling System (ROMS v3.6) implemented in
605 the Coupled Ocean–Atmosphere–Wave–Sediment Transport Modeling System (COAWST
606 r1234). Geoscientific Model Development 11:1849-1871. DOI: 10.5194/gmd-11-1849-2018.

607 Son M. (2009) Flocculation and transport of cohesive sediment, (Ph.D. Dissertation) University of
608 Florida, Gainesville.

609 Strom K., Keyvani A. (2016) Flocculation in a decaying shear field and its implications for mud
610 removal in near‐field river mouth discharges. Journal of Geophysical Research: Oceans
611 121:2142-2162. DOI: 10.1002/2015jc011169.

612 Thomas. D.N., Judd. S.J., Fawcett. N. (1999) Flocculation Modelling: A Review. Water Research
613 33:1579-1592.

614 Verney R., Lafite R., Brun-Cottan J.C., Hir P.L. (2011) Behaviour of a floc population during a tidal
615 cycle: Laboratory experiments and numerical modelling. Continental Shelf Research
616 31:S64-S83.

617 Winterwerp J.C. (1998) A simple model for turbulence induced flocculation of cohesive sediment.
618 Journal of Hydraulic Research 36:309-326.

619 Winterwerp J.C., Kesteren W.G.M.V. (2004) Introduction to the Physics of Cohesive Sediment in the
620 Marine Environment Delft Hydraulics & Delft University of Technology, Delft, Netherlands.

621 Wu J., Liu H., Ren J., Deng J. (2011) Cyclonic Spirals in Tidally Accelerating Bottom Boundary
622 Layers in the Zhujiang (Pearl River) Estuary. Journal of Physical Oceanography
623 41:1209-1226.

624 Xia X.M., Li Y., Yang H., Wu C.Y., Sing T.H., Pong H.K. (2004) Observations on the size and settling
625 velocity distributions of suspended sediment in the Pearl River Estuary, China. Continental
626 Shelf Research 24:1809-1826. DOI: 10.1016/j.csr.2004.06.009.

627 Zhang J., Shen X., Zhang Q., Maa J.P.Y., Qiao G. (2019) Bimodal particle size distributions of
628 fine-grained cohesive sediments in a settling column with oscillating grids. Continental Shelf
629 Research 174:85-94. DOI: 10.1016/j.csr.2019.01.005.

630 Zhang J.F., Zhang Q.H., Qiao G.Q., P.Y J. (2013) Lattice Boltzmann simulation of turbulence-induced
631 flocculation of;cohesive sediment. Ocean Dynamics 63:1123-1135.

632 Zhang W., Didenkulova I., Kurkina O., Cui Y., Haberkerne u., Aepfler R., Santos A.I., Zhang H.,
633 Hanebuth T.J.J. (2018) Internal solitary waves control offshore extension of mud depocenters
634 on the NW Iberian shelf. Marine Geology 409:15-30. DOI: 10.1016/j.margeo.2018.12.008.

635 Zhang Y., Ren J., Zhang W. (2020) Flocculation under the control of shear, concentration and
636 stratification during tidal cycles. Journal of Hydrology 586:124908. DOI:
637 10.1016/j.jhydrol.2020.124908.

638

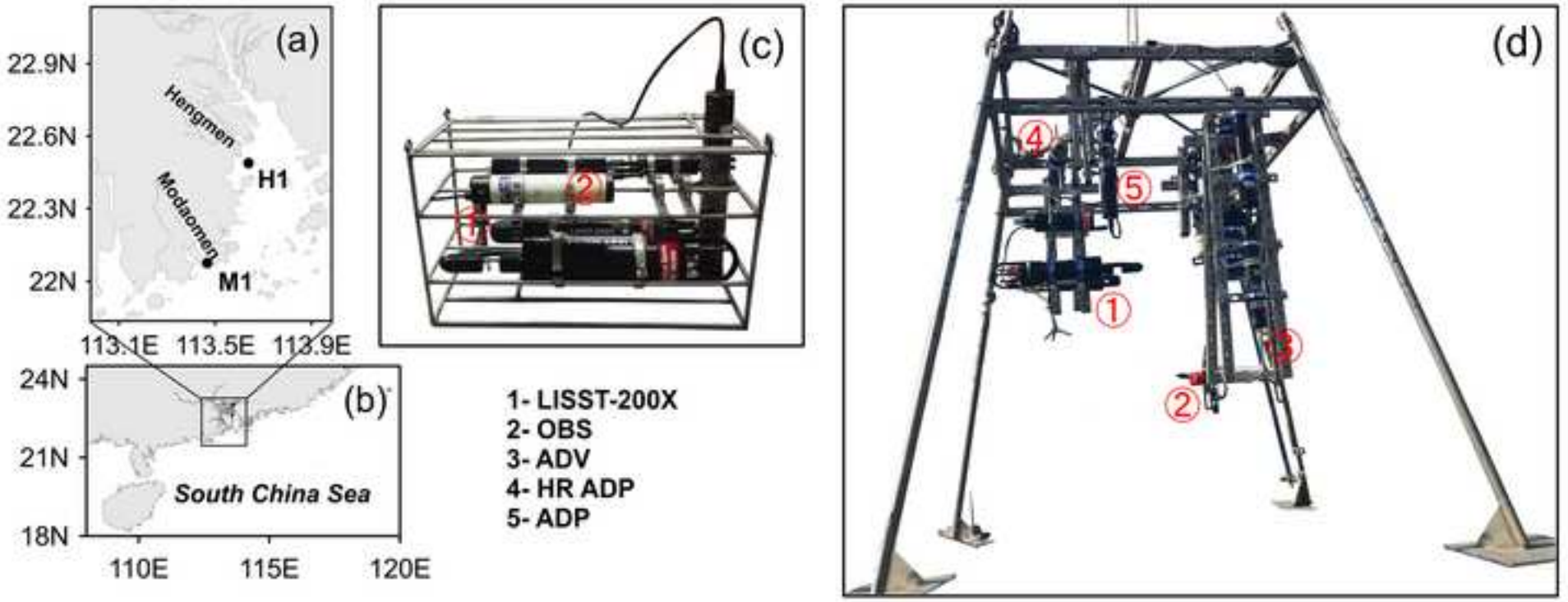

Figure2

Click here to access/download;Figure;Fig2 - Marked.tiff

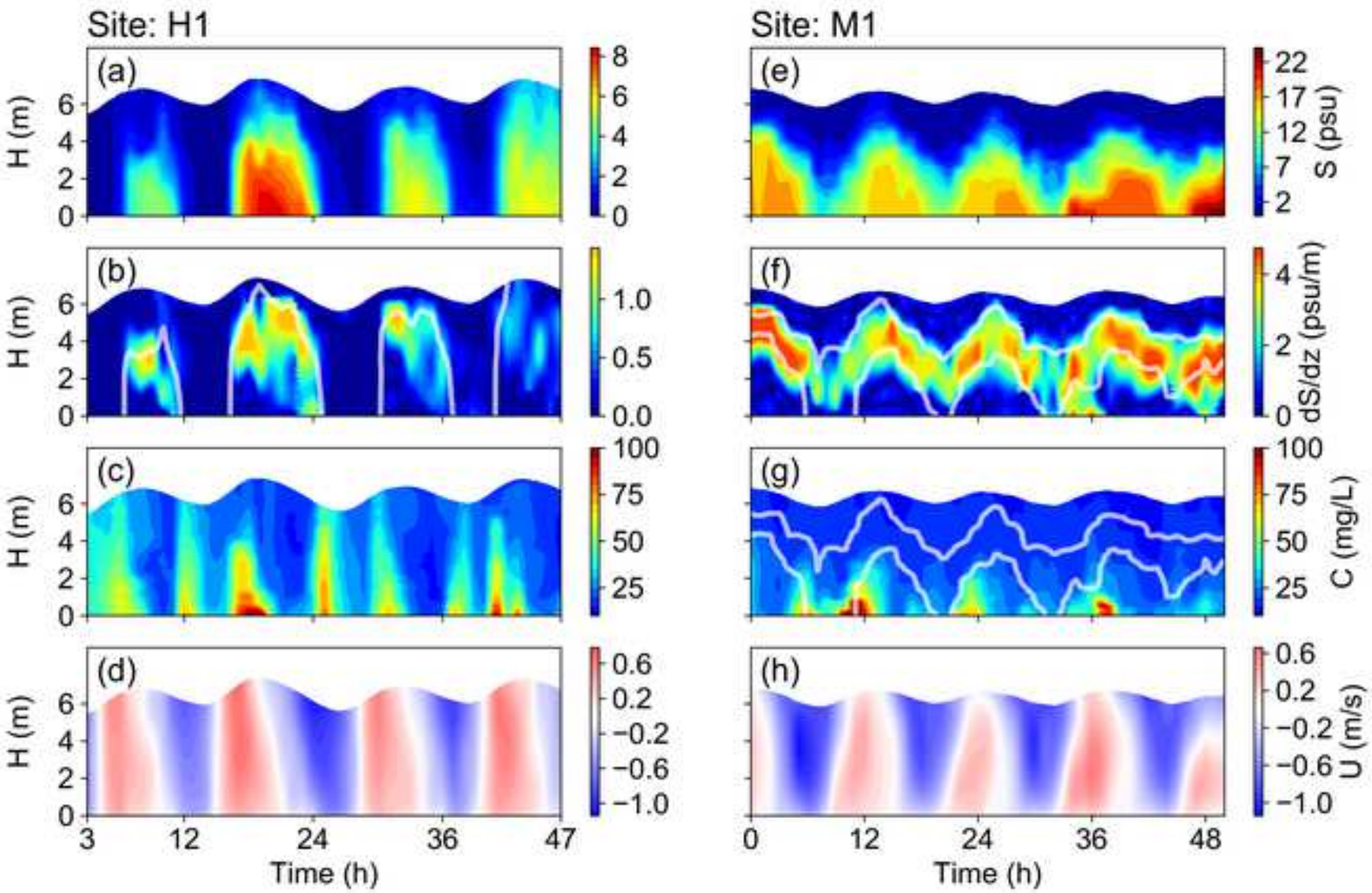

Figure3

Click here to access/download;Figure;Fig3.tiff

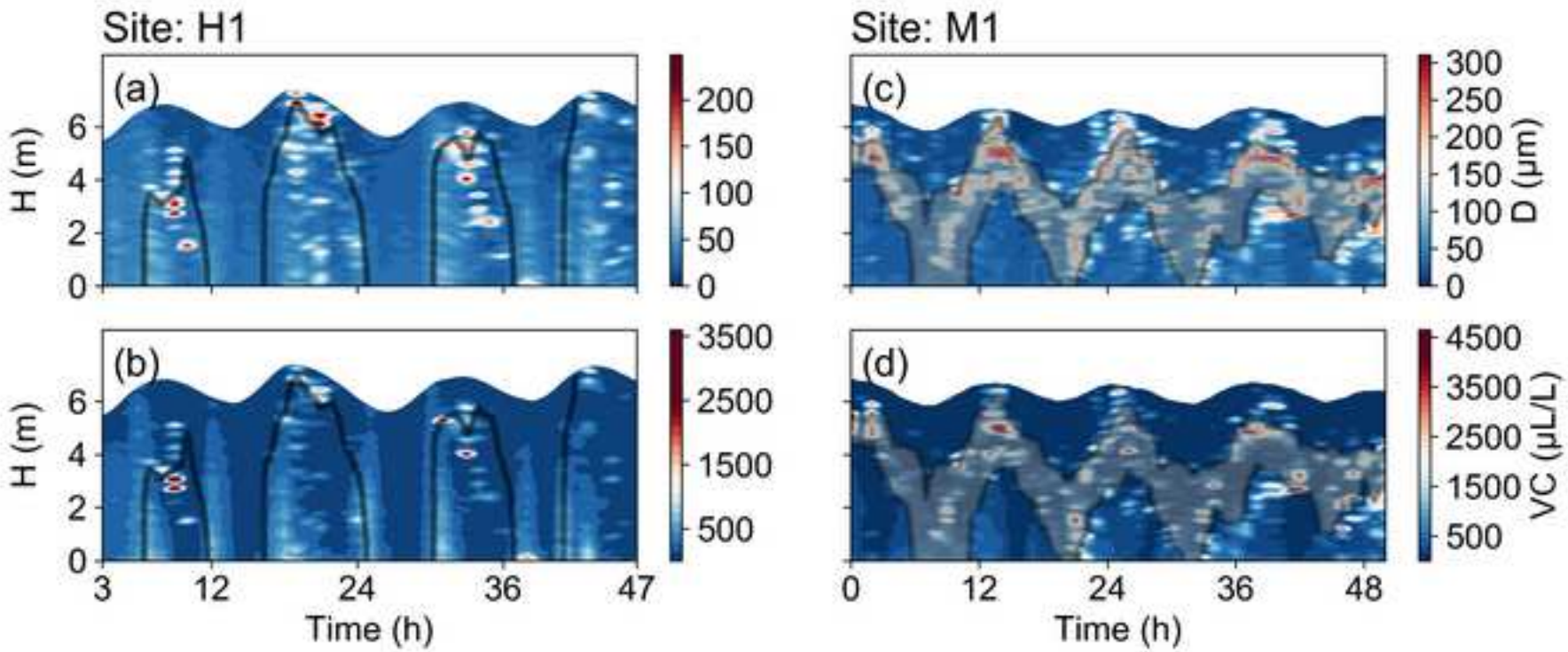

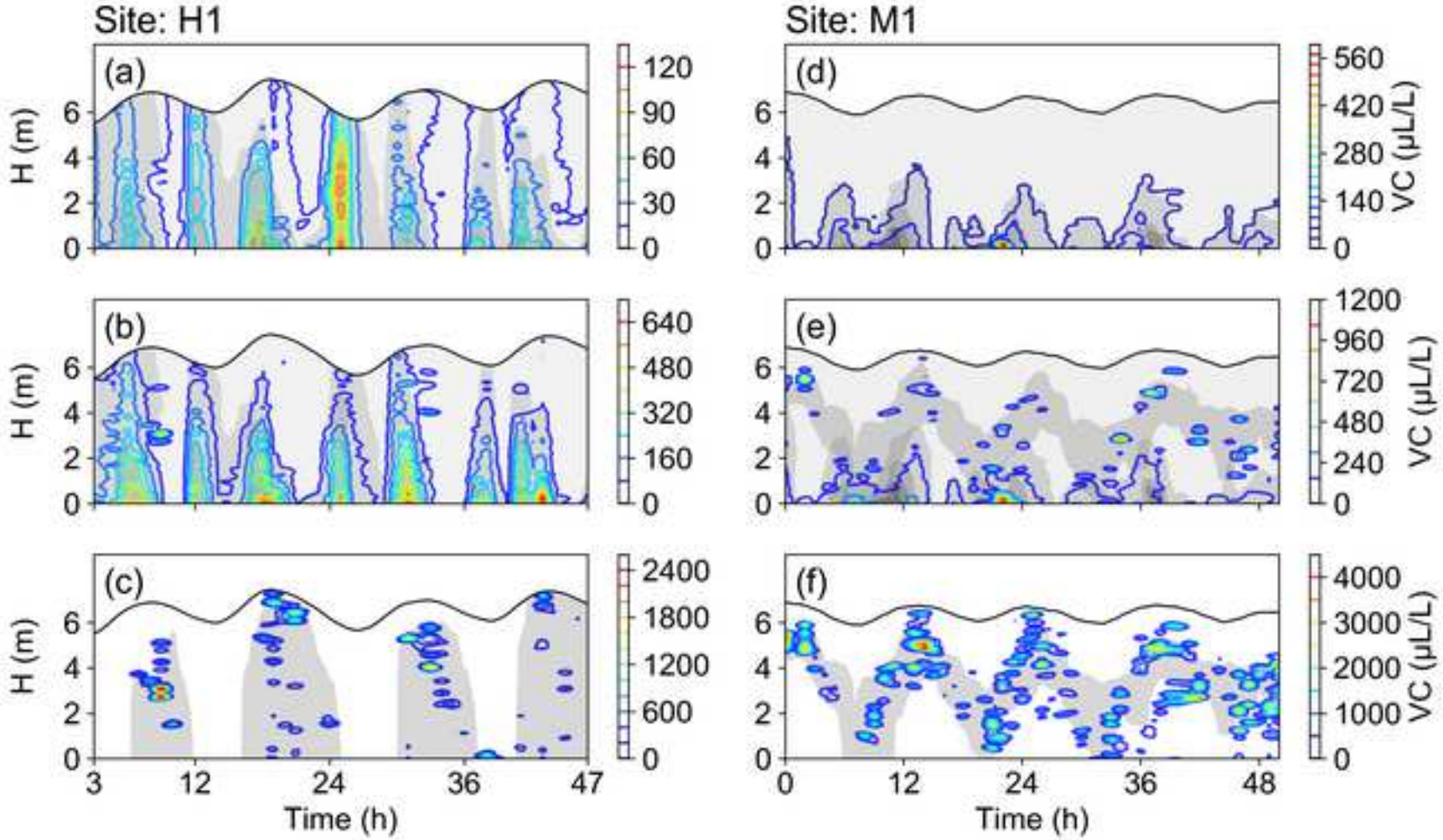

Figure5

Click here to access/download;Figure;Fig5 - Marked.tiff

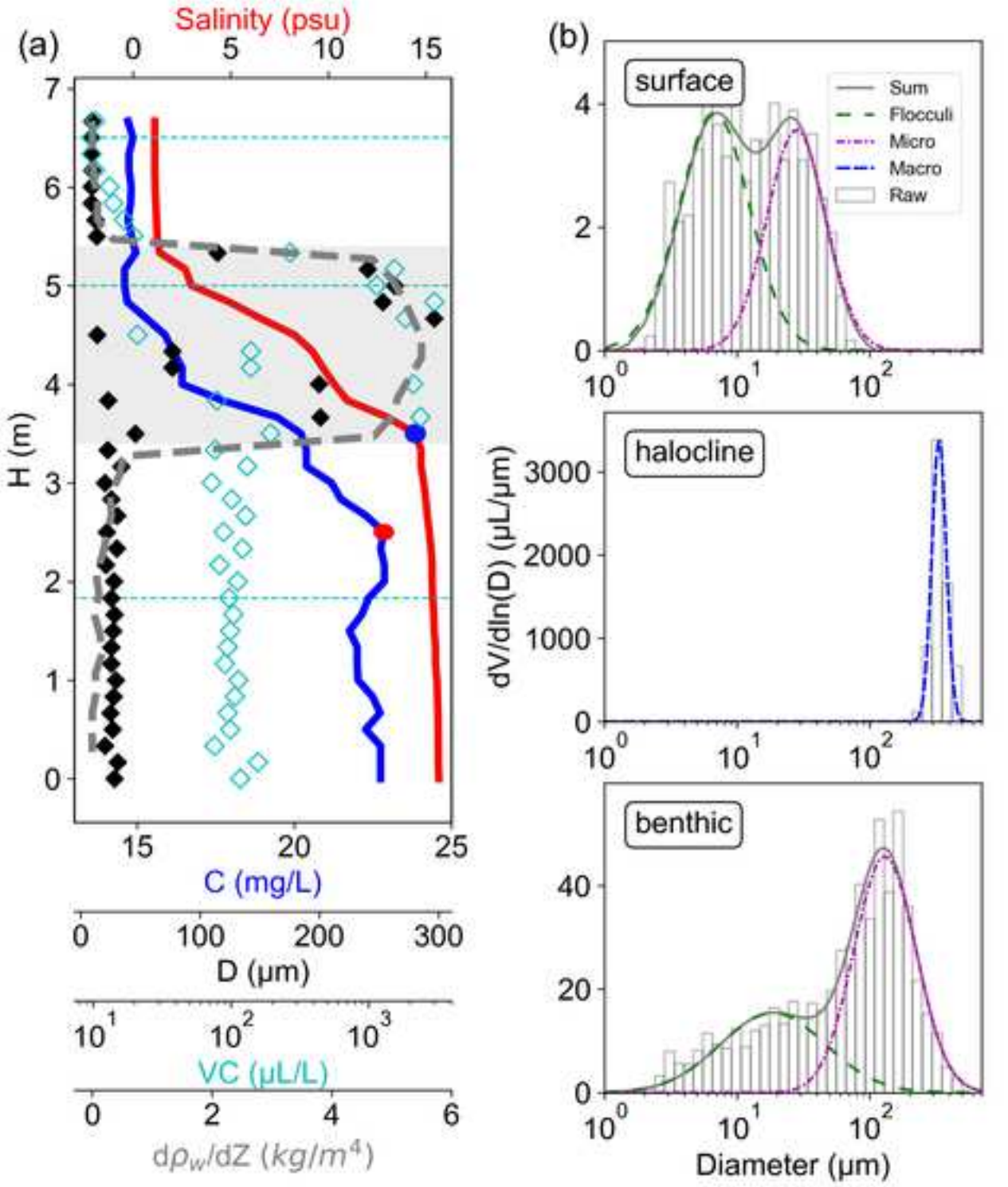

Figure6

Click here to access/download;Figure;Fig6 - Marked.tiff

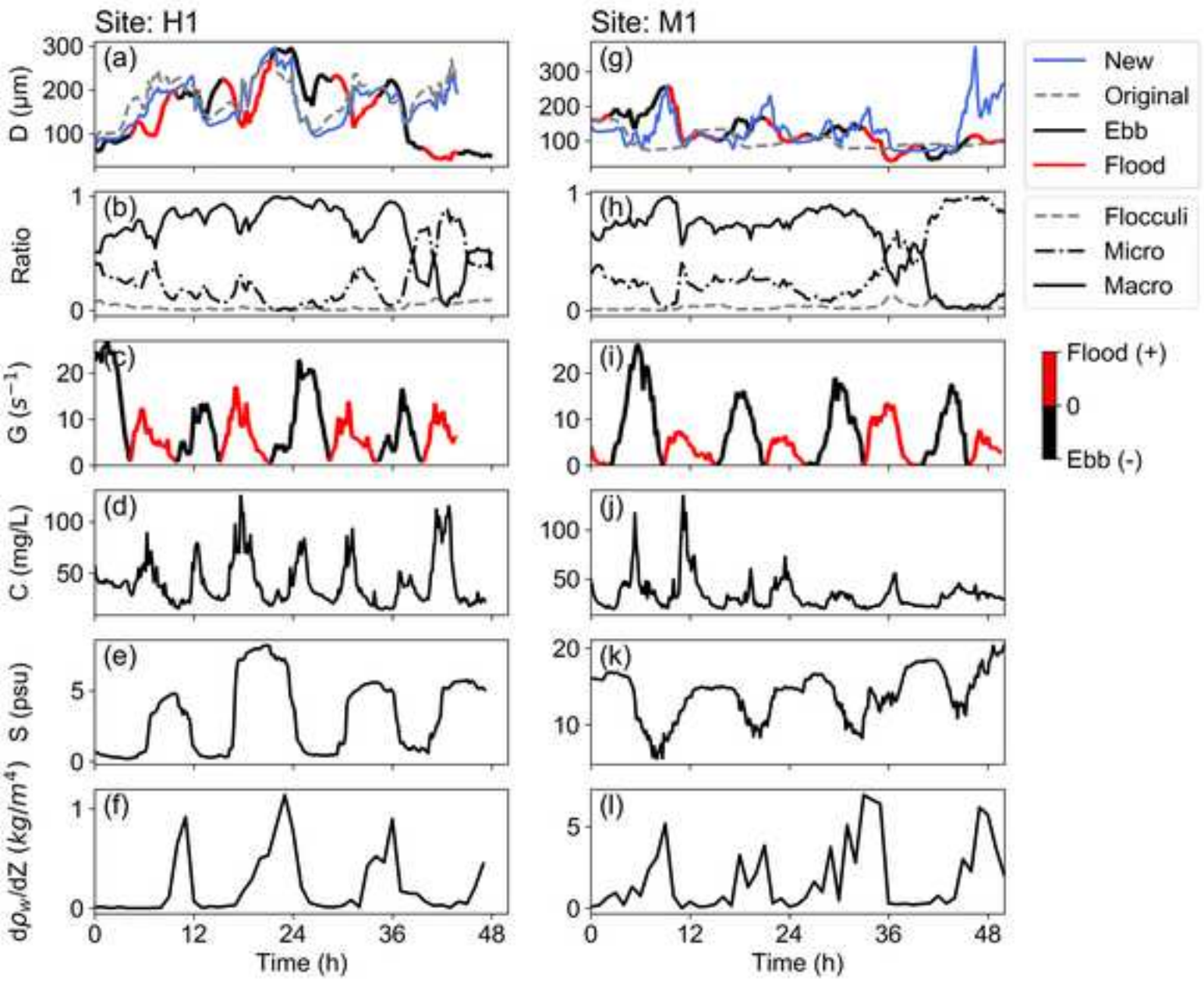

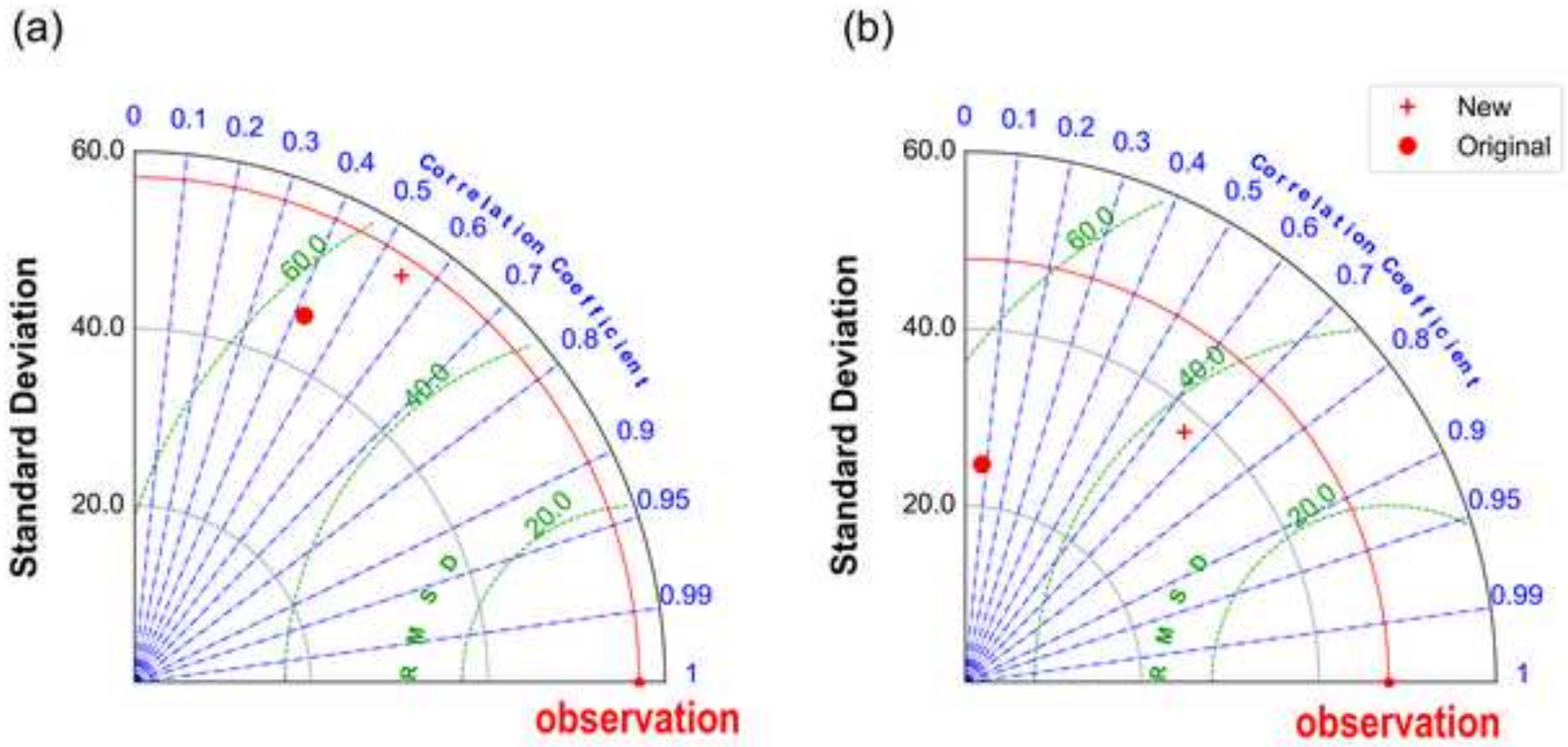

Figure8

Click here to access/download;Figure;Fig8 - Marked.tiff

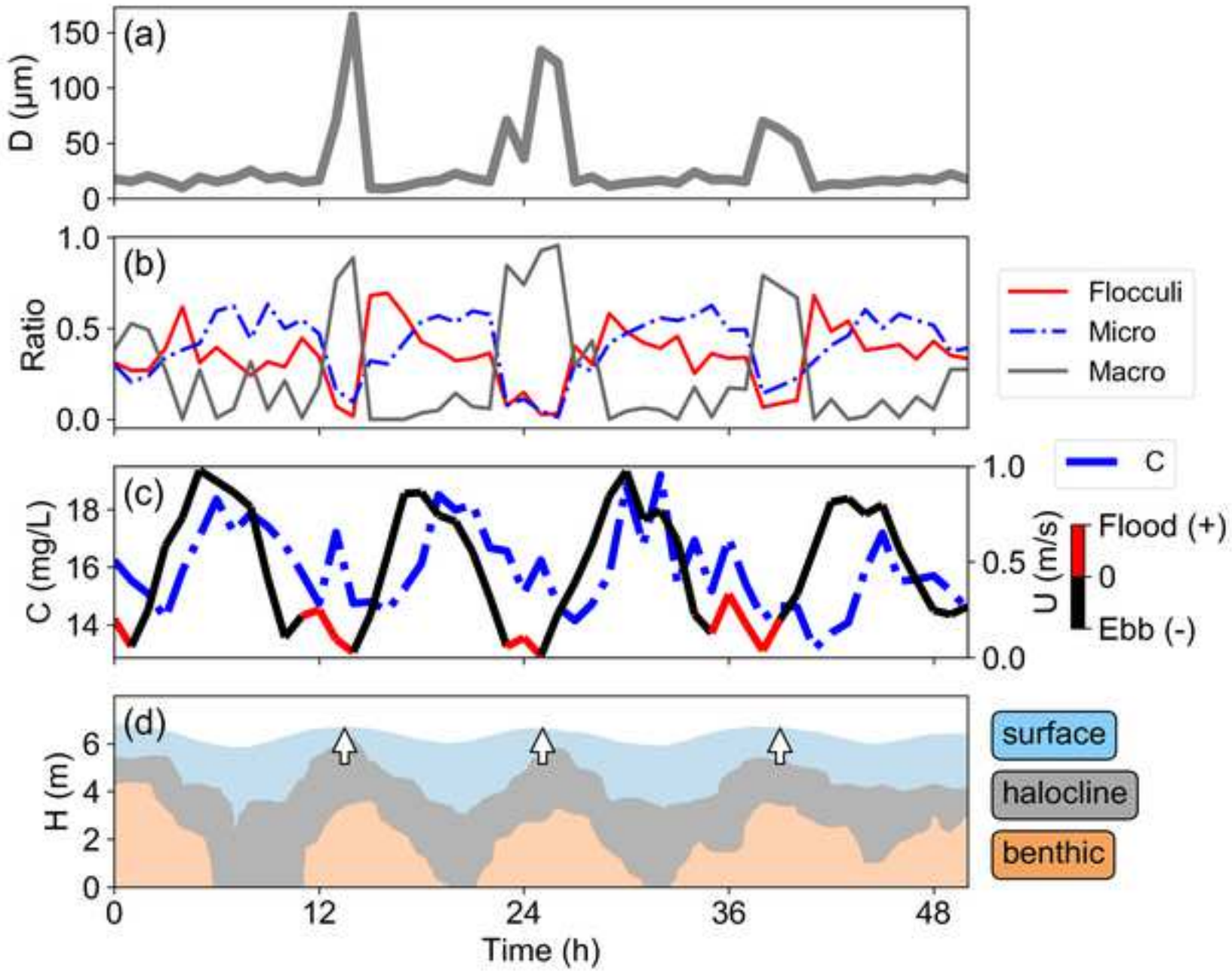

Figure9

Click here to access/download;Figure;Fig9 - Added.tiff

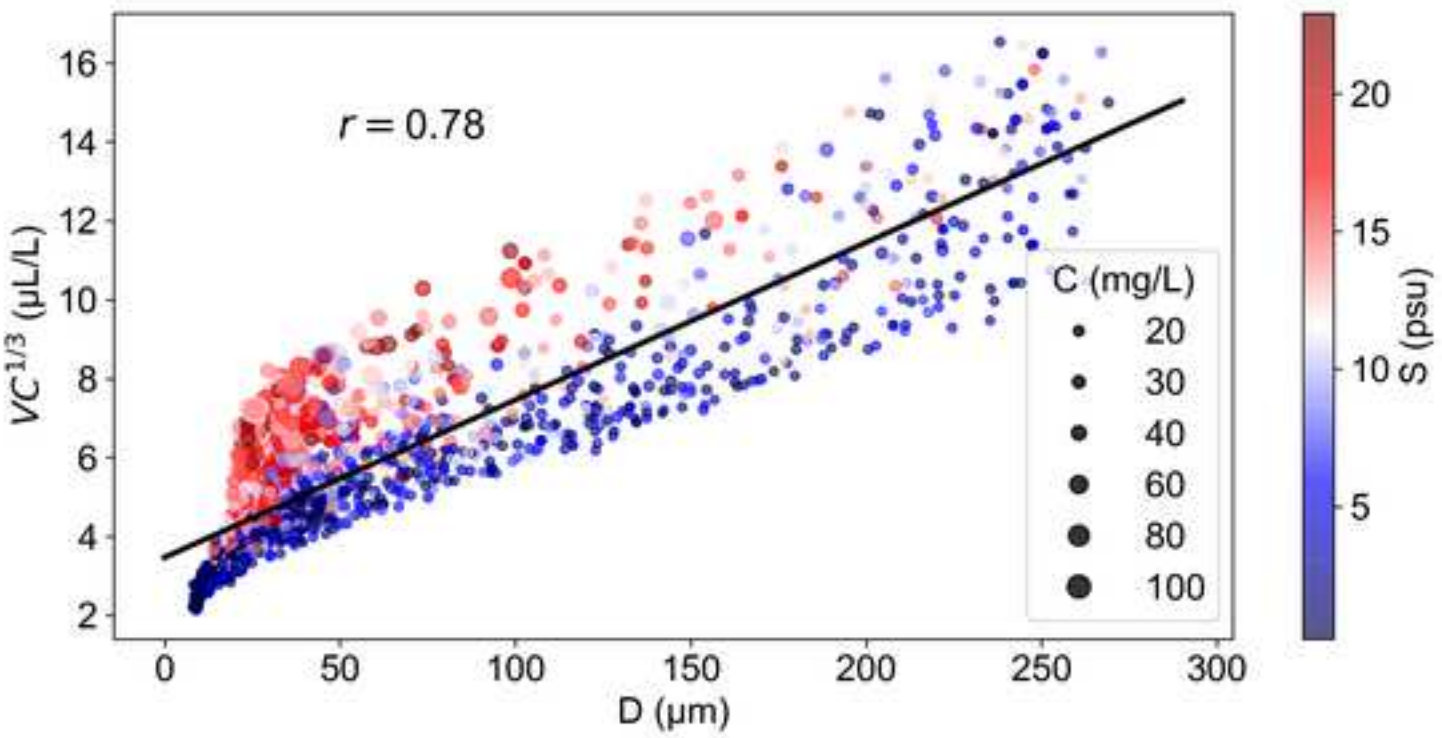

Graphical Abstract (for review)

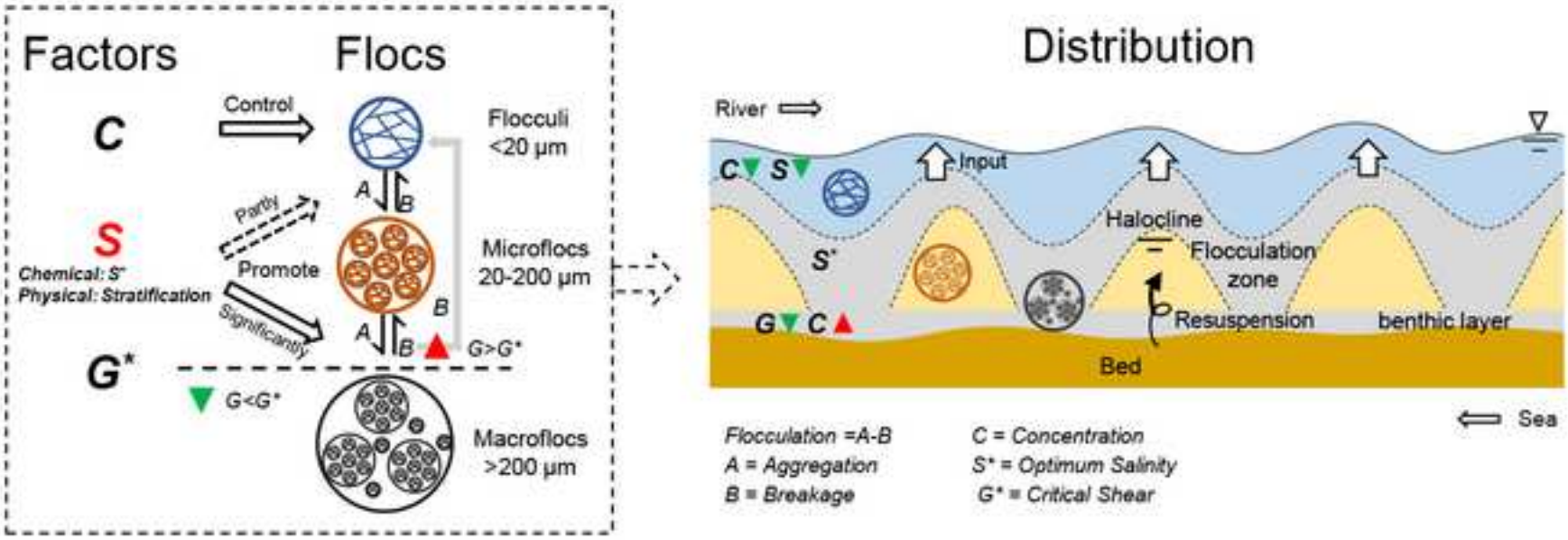

Figure Captions

Fig. 1 Locations of (a) the field survey sites and (b) the study area of the Pearl River Estuary, and instrument packages of (c) steel frame, and (d) benthic quadrupod.

Fig. 2 Times series of (a) and (e) salinity (psu), (b) and (f) salinity gradient (psu/m), (c) and (g) SPM concentration (mg/L), and (d) and (h) axial velocity (m/s) at site H1 (left panels) and site M1 (right panels). Here, "+" and "-" in (d) and (h) indicate ebb (south) and flood (north) flows, respectively, white line in (b) indicates S = 2 psu, and upper and lower lines in (f) and (g) indicate S = 2 and 13 psu, respectively.

Fig. 3 Times series of (a) and (c) flocs diameter (μm), (b) and (d) volumetric concentration (μL/L), at site H1 (left panels) and site M1 (right panels). Here, black lines in (a) and (b) indicate S = 2 psu, and white areas in (c) and (d) indicate S = 2-13 psu.

Fig. 4 Times series of volumetric concentration of (a) and (d) focculi, (b) and (e) microflocs, and (c) and (f) macroflocs at site H1 (left panels) and site M1 (right panels). Here, grey areas in (a), (b), (d) and (e) indicate contour plot of SPM concentration, in (c) indicate S > 2 psu, and in (e) and (f) indicate S = 2-13 psu.

Fig. 5 (a) Profile of flocs diameter (black dots), volumetric concentration (blue dots), the water density gradient (grey line), salinity (red line), and SPM concentration (blue line), and (b) PSDs in the surface, halocline, and benthic layers at t = 15 h in site M1. Here, Flocculi, Micro, Macro, Sum,

and Raw represent the decomposed PSDs of flocculi, microflocs, and macroflocs, the superposition of the decomposed PSDs, and the PSDs measured with the LISST instrument, respectively, and blue dash lines in (a) indicate the corresponding depth of the three layers, at H = 6.5, 5, and 1.8 mab, respectively.

Fig. 6 Times series of (a) and (g) measured and simulated floc diameter, (b) and (h) volumetric percentage of Flocculi, microflocs (Micro), and macroflocs (Macro), (c) and (i) turbulent shear rate, (d) and (j) SPM concentration, (e) and (k) salinity on benthic quadrupod, and (f) and (i) water density gradient at the depth of LISST instrument (1.35 mab) at site H1 (left panels) and M1 (right panels).

Fig. 7 Taylor diagram to assess the model performance against observation at (a) site H1 and (b) M1.

Fig. 8 Times series of (a) flocs diameter and (b) volumetric percentage of Flocculi, microflocs (Micro), and macroflocs (Macro), (c) velocity (U) and SPM concentration (C) in the surface layer, and (d) conceptual three layers at site M1. Here, blue, grey, and yellow areas in (d) indicate $S < 2$, = 2-13, and > 13 psu, respectively.

Fig. 9 The relationship between diameter (D) and the cube root of volumetric concentration (VC).